Dimolybdenum(II) Calixarene Complexes: Synthesis, Structure, Raman Spectroscopy, and Bonding

Jacqueline A. Acho,† Tong Ren,‡ Joanne W. Yun,† and Stephen J. Lippard*,†

Department of Chemistry, Massachusetts Institute of Technology, Cambridge, Massachusetts 02139, and Department of Chemistry, Florida Institute of Technology, Melbourne, Florida 32901

Received March 9, 1995⊗

The preparation of complexes containing metal–metal quadruple bonds supported by calixarene ligands is described. The labile starting materials $[Mo_2(OCCH_3)_2(NCCH_3)_6](BF_4)_2$, a known compound, and $[Mo_2(OCCF_3)_2(NCCH_3)_6](BF_4)_2$ (**1**) were added to solutions of *p-tert*-butylcalix[4]arene and calix[4]arene that were deprotonated with 2 equiv of KH to give, respectively, $[Mo_2(O_2CR)_2(H_2$-*p-tert*-butylcalix[4]arene)] (**2**, **3**: R = CH_3, CF_3) and $[Mo_2(O_2CR)_2(H_2$-calix[4]arene)] (**4**, **5**: R = CH_3, CF_3). The dimolybdenum calixarene products **2**–**5** were studied by ^1H NMR, IR, UV–visible, and Raman spectroscopy. X-ray crystallographic analysis revealed the solid state structure of $2(THF)\cdot C_6H_6$, which contains a molybdenum–molybdenum quadruple bond (2.1263 (6) Å) spanned by two bridging acetate ligands and a tetradentate, doubly-deprotonated calixarene macrocycle. Each Mo–Mo unit is weakly coordinated by an axial THF solvent molecule which is included in the calixarene basket of the neighboring complex. Crystal data: $C_{58}H_{74}O_9Mo_2$, monoclinic, space group $P2_1/c$, a = 12.533 (2) Å, b = 23.515 (2) Å, c = 18.520 (2) Å, β = 95.66 (2)°, V = 5432 (1) Å^3, Z = 4, 6251 unique observed reflections, R = 0.040, R_w = 0.042, T = −73.8 °C. SCF–Xα calculations revealed the nature of the bonding interactions in this new class of compounds.

Introduction

Calixarenes, a class of polyphenolic macrocycles,[1] are receiving increased attention since they are relatively easy to prepare,[2] have host–guest inclusion properties,[3] and coordinate to transition metal ions.[4] Absent from this list of known transition metal calixarene complexes are those having multiple metal–metal bonds, although the calixarenes represent good ligand candidates since many members of this class have been prepared with alkoxide and aryloxide donor ligands.[5] We have therefore undertaken a study to determine the effects of binding a calixarene ligand to a molybdenum–molybdenum quadruple bond and the properties of the resulting complex. The preparation of dimolybdenum(II) calixarene complexes was achieved by allowing the labile starting material $[Mo_2(O_2CCH_3)_2(NCCH_3)_6](BF_4)_2$[6,7] to react with the doubly-deprotonated calix[4]arene and *p-tert*-butylcalix[4]arene macrocycles (Figure 1). Previously we reported the synthesis and structure determination of $[Mo_2(O_2CCH_3)_2(H_2$-*p-tert*-butylcalix[4]arene)].[8] Here we give full details of the structure as well as the preparation of related trifluoroacetate dimolybdenum calixarene products from the new starting material $[Mo_2(O_2CCF_3)_2(NCCH_3)_6](BF_4)_2$. These compounds represent the first examples of a class of calixarene complexes of the metal–metal quadruple bond, the bonding in which was probed by vibrational spectroscopy and by SCF–Xα molecular orbital calculations.

Experimental Section

General Considerations. All synthetic procedures were carried out in a nitrogen-filled drybox or by using standard Schlenk line techniques. Acetonitrile was distilled from CaH_2. All other solvents were distilled under nitrogen from sodium benzophenone ketyl. Calix[4]arene[9] and *p-tert*-butylcalix[4]arene[2a] were prepared according to the literature procedures and dried at 120 °C under vacuum for 24 h. $[Mo_2(O_2CCF_3)_4]$[10] and $[Mo_2(O_2CCH_3)_2(NCCH_3)_6](BF_4)_2$[6,7] were also prepared according to published procedures. Potassium hydride was purchased as a mineral oil suspension from Aldrich and rinsed with pentane prior to use. All other reagents were obtained from commercial sources and used without further purification. NMR spectra were recorded on a Varian XL-300 spectrometer at room temperature. All IR spectra were run on a Bio-Rad FTS7 Fourier transform instrument. UV–visible spectra were recorded on a Hewlett-Packard 8452A diode array spectrophotometer.

Preparation of $[Mo_2(O_2CCF_3)_2(NCCH_3)_6](BF_4)_2$ (1). Yellow crystals of $[Mo_2(O_2CCF_3)_4]$[10] (450 mg, 0.0699 mmol) were added to a

† Massachusetts Institute of Technology.
‡ Florida Institute of Technology.
⊗ Abstract published in *Advance ACS Abstracts,* September 1, 1995.

(1) Gutsche, C. D. *Calixarenes*; The Royal Society of Chemistry: Cambridge, U.K., 1989; Vol. 1.
(2) Preparations of standard calix[4,6,8]arenes: (a) Gutsche, C. D.; Iqbal, M. *Org. Synth.* **1989**, *68*, 234. (b) Gutsche, C. D.; Dhawan, B.; Leonis, M.; Stewart, D. *Org. Synth.* **1989**, *68*, 238. (c) Munch, J. H.; Gutsche, C. D. *Org. Synth.* **1989**, *68*, 243.
(3) For some examples, see: (a) Andreetti, G. D.; Ungaro, R.; Pochini, A. *J. Chem. Soc., Chem. Commun.* **1979**, 1005. (b) McKervey, M. A.; Seward, E. M.; Ferguson, G.; Ruhl, B. L. *J. Org. Chem.* **1986**, *51*, 3581. (c) Bott, S. G.; Coleman, A. W.; Atwood, J. L. *J. Am. Chem. Soc.* **1986**, *108*, 1709. (d) Andreetti, G. D.; Ugozzoli, F.; Ungaro, R.; Pochini, A. In *Inclusion Compounds*; Atwood, J. L., Ed.; Oxford Science: New York, 1984; Vol 4. (e) Atwood, J. L.; Orr, G. W.; Juneja, R. K.; Bott, S. G.; Hamada, F. *Pure Appl. Chem.* **1993**, *65*, 1471.
(4) Examples include: (a) Olmstead, M. M.; Sigel, G.; Hope, H.; Xu, X.; Power, P. P. *J. Am. Chem. Soc.* **1985**, *107*, 8087. (b) Bott, S. G.; Coleman, A. W.; Atwood, J. L. *J. Chem. Soc., Chem. Commun.* **1986**, 610. (c) Hofmeister, G. E.; Hahn, F. E.; Pedersen, S. F. *J. Am. Chem. Soc.* **1989**, *111*, 2318. (d) Hofmeister, G. E.; Alvarado, E.; Leary, J. A.; Yoon, D. I.; Pedersen, S. F. *J. Am. Chem. Soc.* **1990**, *112*, 8843. (e) Corazza, F.; Floriani, C.; Chiesi-Villa, A.; Guastini, C. *J. Chem. Soc., Chem. Commun.* **1990**, 640. (f) Corazza, F.; Floriani, C.; Chiesi-Villa, A.; Guastini, C. *J. Chem. Soc., Chem. Commun.* **1990**, 1083. (g) Corazza, F.; Floriani, C.; Chiesi-Villa, A.; Rizzoli, C. *Inorg. Chem.* **1991**, *30*, 4465.
(5) Cotton, F. A.; Walton, R. A. *Multiple Bonds Between Metal Atoms*, 2nd ed.; Oxford University Press: New York, 1993.
(6) Cotton, F. A.; Reid, A. H., Jr.; Schwotzer, W. *Inorg. Chem.* **1985**, *24*, 3965.
(7) Pimblett, G.; Garner, C. D.; Clegg, W. *J. Chem. Soc., Dalton Trans.* **1986**, 1257.
(8) Acho, J. A.; Lippard, S. J. *Inorg. Chim. Acta* **1995**, *229*, 5.
(9) Gutsche, C. D.; Levine, J. A.; Sujeeth, P. K. *J. Org. Chem.* **1985**, *50*, 5802.
(10) Cotton, F. A.; Norman, J. G., Jr. *J. Coord. Chem.* **1971**, *1*, 161.

0020-1669/95/1334-5226$09.00/0

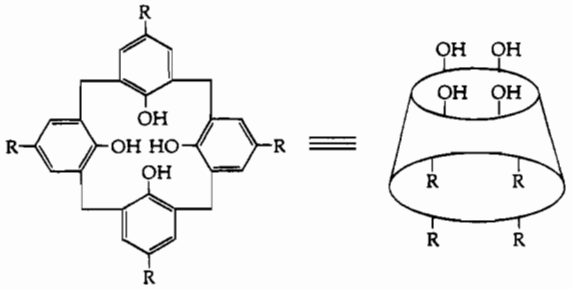

Figure 1. Two representations of calix[4]arenes (calix[4]arene for R = H, and *p-tert*-butylcalix[4]arene for R = *tert*-butyl).

solution of Me_3OBF_4 (207 mg, 1.399 mmol) in 15 mL of acetonitrile. As the yellow solids dissolved, the reaction mixture turned orange in color, then red-orange, and then pink. The reaction solution was allowed to stir for 20 h. The solvent was then removed in vacuo, and the crude product was washed with 10 mL of DME to remove any residual starting materials. The insoluble pink solids were collected on a fritted funnel, rinsed twice with 10 mL of pentane, and vacuum dried to give 426 mg (0.508 mmol, 73% yield) of the pink product **1**. The resulting powder was judged to be >95% pure by ^{1}H NMR spectroscopy and could be further recrystallized from hot acetonitrile. Anal. Calcd for $C_{14}H_{15}N_5O_4B_2F_{14}Mo_2$ (**1**·$NCCH_3$): C, 21.10; H, 1.90; N, 8.79. Found: C, 20.74; H, 1.92; N, 8.48. IR (CsI, Nujol): 2323 (s), 2294 (s), 1599 (s), 1377 (m), 1241 (s), 1196 (vs), 1077 (vs, ν_{B-F}), 1027 (s), 954 (m), 867 (m), 776 (m), 736 (s), 526 (m), 316 (w) cm^{-1}. ^{1}H NMR ($NCCD_3$, 300 MHz): δ 1.96 (s, Mo−$NCCH_3$) ppm. UV−vis (THF) (λ_{max}, nm (ϵ, M^{-1}cm^{-1})): 382 (440), 528 (857).

Preparation of [$Mo_2(O_2CCH_3)_2$(H$_2$-*p-tert*-butylcalix[4]arene)] (2). This compound was prepared in 73% yield and purified as indicated in ref 8. Anal. Calcd for $C_{48}H_{60}O_8Mo_2$ (**2**): C, 60.25; H, 6.32. Found: C, 59.99; H, 6.15. IR (CsI, Nujol): 1304 (s), 1267 (m), 1205 (s), 1042 (m), 872 (m), 824 (m), 788 (m), 745 (m), 680 (m), 618 (w), 527 (w), 478 (w), 381 (w), 343 (w), 309 (w) cm^{-1}. Raman (THF): 378 cm^{-1} (ν_{Mo-Mo}). ^{1}H NMR (THF-d_8, 300 MHz): δ 1.26 (s, 36 H; *t*-Bu), 1.78 (br, 8 H; *axial* THF), 2.57 (d, J = 12 Hz, 2 H; CH_2), 2.92 (s, 6 H; O_2CCH_3), 3.07 (d, J = 12 Hz, 2 H; CH_2), 3.75 (d, J = 12 Hz, 2 H; CH_2), 3.63 (br, 8 H; *axial* THF), 4.57 (d, J = 12 Hz, 2 H; CH_2), 7.13 (dd, J = 12 Hz, 3 Hz, 8 H; Ph), 16.94 (s, 2 H; Mo−OHPh) ppm. UV−vis (THF) (λ_{max}, nm (ϵ, M^{-1} cm^{-1})): 379 (1213), 514 (875).

Preparation of [$Mo_2(O_2CCF_3)_2$(H$_2$-*p-tert*-butylcalix[4]arene)] (3). *p-tert*-Butylcalix[4]arene (100 mg, 0.135 mmol) was stirred vigorously with 2 equiv of KH (11 mg, 0.274 mmol) in 15 mL of THF for 2 h. To the resulting clear, colorless solution was added solid pink [$Mo_2(O_2CCF_3)_2(NCCH_3)_6$]($BF_4$)$_2$ (**1**) (113 mg, 0.135 mmol). The reaction suspension was stirred overnight, during which time the solids disappeared and a dark red-orange color developed. The solvent was removed in vacuo, and the product was extracted with pentane. The pentane extract was filtered through Celite and concentrated to dryness. Recrystallization from pentane with a few drops of THF afforded orange-pink crystals of **3** in 39% yield (56 mg, 0.052 mmol). Anal. Calcd for $C_{48}H_{54}O_8F_6Mo_2$ (**3**): C, 54.14; H, 5.11. Found: C, 54.02; H, 5.14. IR (CsI, Nujol): 1598 (m), 1305 (m), 1265 (w), 1195 (s), 1161 (m), 1128 (m), 1033 (m), 969 (m), 923 (m), 911 (m), 870 (m), 824 (m), 732 (s), 619 (w), 557 (w), 358 (w) cm^{-1}. Raman (THF): 360 cm^{-1} (ν_{Mo-Mo}). ^{1}H NMR (THF-d_8, 300 MHz): δ 1.22 (s, 36 H; *t*-Bu), 1.78 (br, 8 H; *axial* THF), 2.54 (d, J = 12 Hz, 2 H; CH_2), 3.08 (d, J = 12 Hz, 2 H; CH_2), 3.63 (br, 8 H; *axial* THF), 3.81 (d, J = 12 Hz, 2 H; CH_2), 4.51 (d, J = 12 Hz, 2 H; CH_2), 7.16 (s, 8 H; Ph), 16.96 (s, 2 H; Mo−OHPh) ppm. UV−vis (THF) (λ_{max}, nm (ϵ, M^{-1} cm^{-1})): 338 (4396), 414 (3049), 530 (1005).

Preparation of [$Mo_2(O_2CCH_3)_2$(H$_2$-calix[4]arene)] (4). This compound was prepared in 69% yield and purified as indicated in ref 8. Anal. Calcd for $C_{32}H_{28}O_8Mo_2$ (**1**): C, 52.47; H, 3.85. Found: C, 52.47; H, 4.27. IR (CsI, Nujol): 1594 (w), 1298 (m), 1262 (m), 1218 (m), 1100 (sh), 1076 (m), 1029 (m), 968 (m), 891 (m), 856 (m), 824 (m), 745 (m), 727 (m), 676 (m), 613 (w), 580 (w), 472 (w), 464 (w), 376 (w), 340 (w) cm^{-1}. Raman (THF): 379 cm^{-1} (ν_{Mo-Mo}). ^{1}H NMR (THF-d_8, 300 MHz): δ 1.78 (br, 8 H; *axial* THF), 2.55 (s, J = 12 Hz, 2 H; CH_2), 2.89 (s, 6 H; O_2CCH_3), 3.04 (d, J = 12 Hz, 2 H; CH_2), 3.63 (br, 8 H; *axial* THF), 3.72 (d, J = 12 Hz, 2 H; CH_2), 4.54 (d, J = 12 Hz, 2 H; CH_2), 6.55 (t, J = 6 Hz, 4 H; Ph), 7.06 (d, J = 6 Hz, 8 H Ph), 16.94 (s, 2 H; Mo−OHPh) ppm. UV−vis (THF) (λ_{max}, nm (ϵ, M^{-1} cm^{-1})): 380 (712), 512 (591).

Table 1. X-ray Crystallographic Information for [$Mo_2(O_2CCH_3)_2$(H$_2$-*p-tert*-butylcalix[4]arene)(THF)]·C_6H_6 (**2**(THF)·C_6H_6)[a]

formula	$C_{58}H_{74}O_9Mo_2$	2θ limits (deg)	3−50
a (Å)	12.533 (2)	data limits	+h+k±l
b (Å)	23.515 (3)	μ (cm^{-1})	5.14
c (Å)	18.520 (2)	no. of total data	10775
β (deg)	95.66 (2)	no. of unique data	9787
V (Å^3)	5432 (1)	R(merge)[b]	3.6
T (°C)	−73.8	no. of unique obsd[c] data	6251
fw	1107.10	no. of LS params	630
Z	4	p factor	0.03
ϱ_{calc} (g/cm^3)	1.35	R[d]	0.040
space group	$P2_1/c$	R_w	0.042

[a] Data were collected on an Enraf-Nonius CAD-4F κ geometry diffractometer using Mo Kα radiation. [b] R(merge) = $\sum_{i=1}^{n}\sum_{j=1}^{m}|\langle F_i^2\rangle - F_{ij}^2|/\sum_{i=1}^{n}mX\langle F_i^2\rangle$, where n = number of reflections observed more than once, m = number of times a given reflection was observed, and $\langle F_i^2\rangle$ is the average value of F^2 for reflection i. [c] Observation criterion $I > 3\sigma(I)$. [d] $R = \sum||F_o| - |F_c||/\sum|F_o|$, $R_w = [\sum w(|F_o| - |F_c|)^2/\sum w|F_o|^2]^{1/2}$, where $w = 1/\sigma(F)$, as defined in ref 11.

Preparation of [$Mo_2(O_2CCF_3)_2$(H$_2$-calix[4]arene)] (5). To a stirred solution of calix[4]arene (100 mg, 0.236 mmol) in 15 mL of THF was added 2 equiv of KH (19 mg, 0.474 mmol). The effervescent solution was allowed to react for at least 2 h before solid pink [$Mo_2(O_2CCF_3)_2(NCCH_3)_6$]($BF_4$)$_2$ (**1**) (198 mg, 0.236 mmol) was added. The pink solid disappeared and a red-orange color developed as the reaction was stirred overnight. The solvent was then removed in vacuo and the product extracted with pentane. Concentrating the pentane solution to dryness produced bright orange microcrystals in 71% yield (140 mg, 0.166 mmol). Larger crystals could be grown by slow diffusion of pentane into a toluene solution of **5** with a few drops of THF. Anal. Calcd for $C_{48}H_{54}O_{12}F_6Mo_2$ (**5**·4THF): C, 51.07; H, 4.82. Found: C, 51.20; H, 4.48. IR (CsI, Nujol): 1605 (s), 1377 (m), 1367 (sh), 1296 (w), 1263 (m), 1196 (vs), 1163 (s), 1100 (m), 1034 (m), 968 (m), 858 (m), 825 (w), 752 (s), 732 (vs), 668 (w), 613 (w), 581 (w), 547 (w), 499 (w), 472 (w), 358 (w) cm^{-1}. Raman (THF): 357 cm^{-1} (ν_{Mo-Mo}). ^{1}H NMR (THF-d_8, 300 MHz): δ 1.78 (br, 8 H; *axial* THF), 2.55 (d, J = 12 Hz, 2 H; CH_2), 3.10 (d, J = 12 Hz, 2 H; CH_2), 3.63 (br, 8 H; *axial* THF), 3.83 (d, J = 12 Hz, 2 H; CH_2), 4.53 (d, J = 12 Hz, 2 H; CH_2), 6.65 (t, J = 6 Hz, 4 H; Ph), 7.13 (d, J = 6 Hz, 8 H; Ph), 17.00 (s, 2 H; Mo−OHPh) ppm. UV−vis (THF) (λ_{max}, nm (ϵ, M^{-1} cm^{-1})): 338 (4056), 412 (2220), 528 (716).

X-ray Crystallography. [$Mo_2(O_2CCH_3)_2$(H$_2$-*p-tert*-butylcalix[4]-arene)(THF)]·C_6H_6, (2(THF)·C_6H_6). Air-sensitive X-ray quality crystals of **2**(THF)·C_6H_6 were grown by slow evaporation of pentane into a benzene solution of **2** containing a few drops of THF. A bright red-orange block of dimensions 0.5 × 0.4 × 0.15 mm was mounted on a quartz fiber from a liquid nitrogen cold stage and studied on an Enraf-Nonius CAD4 diffractometer at −73.8 °C by methods commonly employed in our laboratory,[11] details of which are provided in Table 1. Unit cell parameters were determined from 25 reflections with 20° < 2θ < 30°. Crystal quality was judged to be acceptable by open counter ω-scans of several low-angle reflections ($\Delta\overline{\omega_{1/2}}$ = 0.27°, no fine structure) and axial photographs. Systematic absences and intensity statistics were consistent with the monoclinic space group $P2_1/c$. The structure was solved by conventional direct methods and refined by full matrix least-squares procedures. All non-hydrogen atoms were refined anisotropically, and the phenol hydrogen atoms, H(1) and H(2), were located on a difference Fourier map and allowed to refine isotropically. Other hydrogen atoms were calculated and fixed on the attached carbon atoms (d_{C-H} = 0.95 Å, B_H = 1.2B_C). Lorentz and polarization corrections were applied, as was an empirical absorption correction based on ψ scans. The largest residual peak in the final difference Fourier map was 0.7 e$^-$/Å^3, at a distance of 1.04 Å from

(11) Carnahan, E. M.; Rardin, R. L.; Bott, S. G.; Lippard, S. J. *Inorg. Chem.* **1992**, *31*, 5193.

Table 2. Final Positional Parameters and B(eq) for $[Mo_2(O_2CCH_3)_2(H_2$-*p*-*tert*-butylcalix[4]arene)(THF)]·C_6H_6 (**2**)(THF)·C_6H_6[a]

atom	*x*	*y*	*z*	*B*(eq),[b] (Å^2)	atom	*x*	*y*	*z*	*B*(eq),[b] (Å^2)
Mo(1)	0.076 149(33)	0.427 805(17)	1.496 705(21)	1.82(2)	C(50)	0.481 42(52)	0.133 56(28)	1.679 93(36)	5.2(3)
Mo(2)	0.124 205(32)	0.359 315(17)	1.432 370(21)	1.77(2)	C(60)	0.253 87(38)	0.423 08(19)	1.642 71(25)	2.1(2)
O(2)	−0.017 14(25)	0.366 07(13)	1.363 96(16)	2.2(1)	C(61)	0.360 17(38)	0.408 24(19)	1.661 16(25)	2.1(2)
O(4)	0.204 71(25)	0.416 14(13)	1.369 49(16)	2.2(1)	C(62)	0.400 53(39)	0.410 29(21)	1.733 76(27)	2.6(2)
O(6)	0.150 26(25)	0.487 36(13)	1.435 19(16)	2.2(1)	C(63)	0.338 90(40)	0.427 07(20)	1.788 54(25)	2.4(2)
O(8)	−0.067 22(25)	0.437 43(13)	1.430 96(16)	2.2(1)	C(64)	0.233 11(40)	0.439 88(19)	1.767 75(24)	2.2(2)
O(20)	0.042 72(24)	0.297 12(13)	1.491 81(17)	1.9(1)	C(65)	0.186 77(38)	0.438 64(19)	1.696 09(24)	2.1(2)
O(40)	0.271 19(25)	0.344 97(13)	1.499 19(17)	2.1(1)	C(66)	0.069 48(37)	0.452 25(19)	1.679 36(24)	2.0(2)
O(60)	0.216 62(24)	0.423 37(13)	1.570 12(16)	2.0(1)	C(67)	0.389 71(45)	0.429 56(26)	1.867 36(26)	3.5(3)
O(80)	−0.006 33(25)	0.374 68(13)	1.564 07(16)	2.2(1)	C(68)	0.478 86(59)	0.474 12(33)	1.873 06(33)	6.1(4)
O(100)	0.171 39(26)	0.298 36(14)	1.326 04(17)	2.5(1)	C(69)	0.309 11(54)	0.443 54(30)	1.919 98(29)	5.0(3)
C(1)	−0.085 15(38)	0.403 70(20)	1.377 39(25)	2.2(2)	C(70)	0.439 10(49)	0.371 35(31)	1.888 29(31)	4.8(3)
C(2)	−0.189 13(42)	0.406 92(23)	1.331 37(28)	3.2(2)	C(80)	−0.033 80(34)	0.364 83(20)	1.632 62(23)	1.8(2)
C(3)	0.201 10(38)	0.468 44(21)	1.383 98(24)	2.2(2)	C(81)	−0.003 81(35)	0.402 53(19)	1.688 95(24)	1.8(2)
C(4)	0.259 25(41)	0.510 04(22)	1.339 87(27)	2.9(2)	C(82)	−0.040 40(37)	0.391 92(20)	1.756 31(24)	2.2(2)
C(20)	0.050 49(38)	0.245 51(19)	1.526 83(23)	2.0(2)	C(83)	−0.104 24(36)	0.345 46(20)	1.769 89(24)	2.1(2)
C(21)	−0.030 45(37)	0.231 58(19)	1.571 43(24)	2.0(2)	C(84)	−0.127 60(36)	0.307 58(20)	1.712 10(26)	2.1(2)
C(22)	−0.027 10(39)	0.178 46(20)	1.603 41(24)	2.2(2)	C(85)	−0.093 63(35)	0.316 44(20)	1.643 87(24)	1.9(2)
C(23)	0.052 32(40)	0.138 85(20)	1.593 39(24)	2.3(2)	C(86)	−0.119 56(37)	0.273 21(20)	1.583 87(25)	2.3(2)
C(24)	0.131 56(38)	0.155 40(19)	1.550 49(24)	2.1(2)	C(87)	−0.153 52(40)	0.338 22(23)	1.841 92(26)	2.7(2)
C(25)	0.133 02(35)	0.208 35(19)	1.517 19(23)	1.9(2)	C(88)	−0.263 35(54)	0.366 94(36)	1.833 97(35)	6.5(4)
C(26)	0.225 93(38)	0.223 86(19)	1.474 92(25)	2.1(2)	C(89)	−0.167 32(52)	0.275 56(25)	1.861 72(29)	4.2(3)
C(27)	0.050 94(46)	0.079 57(21)	1.627 57(27)	2.9(2)	C(90)	−0.084 68(53)	0.365 93(25)	1.904 21(28)	4.1(3)
C(28)	−0.048 19(71)	0.048 85(29)	1.599 74(45)	8.5(5)	C(101)	0.101 76(44)	0.257 51(23)	1.286 50(30)	3.5(3)
C(29)	0.145 40(75)	0.044 07(31)	1.611 40(52)	9.1(5)	C(102)	0.170 45(57)	0.227 52(34)	1.237 08(45)	7.1(4)
C(30)	0.059 00(78)	0.084 45(28)	1.708 32(37)	7.4(4)	C(103)	0.266 51(73)	0.252 65(37)	1.242 41(52)	9.5(6)
C(40)	0.334 40(36)	0.305 25(19)	1.537 04(24)	1.9(2)	C(104)	0.274 59(43)	0.295 27(24)	1.301 17(31)	3.7(3)
C(41)	0.318 87(36)	0.246 78(19)	1.524 04(24)	1.8(2)	C(200)	0.641 87(51)	0.054 47(28)	0.965 05(34)	4.5(3)
C(42)	0.389 61(39)	0.209 55(19)	1.561 66(26)	2.4(2)	C(201)	0.684 47(47)	0.103 93(31)	0.993 23(33)	4.5(3)
C(43)	0.472 04(38)	0.226 37(21)	1.612 32(27)	2.5(2)	C(202)	0.631 77(53)	0.154 66(29)	0.976 04(35)	4.6(3)
C(44)	0.483 01(36)	0.284 31(22)	1.624 09(25)	2.4(2)	C(203)	0.539 54(53)	0.154 55(28)	0.931 72(36)	4.7(3)
C(45)	0.416 23(37)	0.323 94(20)	1.587 40(25)	2.1(2)	C(204)	0.497 21(50)	0.104 39(30)	0.903 48(35)	4.9(3)
C(46)	0.430 72(37)	0.386 87(20)	1.604 67(25)	2.2(2)	C(205)	0.549 70(53)	0.054 24(28)	0.919 87(35)	4.8(3)
C(47)	0.545 84(44)	0.182 38(24)	1.651 64(32)	3.5(3)	H(1)	0.014 2(42)	0.329 4(23)	1.525 3(28)	5(1)
C(48)	0.619 06(54)	0.157 12(32)	1.598 50(42)	6.3(4)	H(2)	0.258 9(39)	0.377 7(21)	1.530 7(26)	3(1)
C(49)	0.613 46(74)	0.207 58(31)	1.714 37(47)	9.7(5)					

[a] Numbers in parentheses are estimated standard deviations of the last significant figure. See Figure 2 for atom labeling scheme. [b] $B_{eq} = {}^4/_3[a^2\beta_{11} + b^2\beta_{22} + c^2\beta_{33} + 2ab\cos(\gamma)\beta_{12} + 2ac\cos(\beta)\beta_{13} + 2bc\cos(\alpha)\beta_{23}]$.

Mo(2). Positional and thermal parameters for non-hydrogen atoms, H(1), and H(2), are given in Table 2.

Raman Spectroscopy. Resonance Raman spectra were obtained by using a Coherent Innova 70 argon ion laser (λ_0 = 514.5 nm). A 0.6-m single monochromator (1200 groove/mm grating), with an entrance slit of 400 μm, and an optical multichannel analyzer were employed in a standard backscattering configuration. A holographic notch filter was used to attenuate Rayleigh scattering. The samples were 0.14 M solutions in THF. Spectra were recorded at room temperature with 200−500 mW of power, while spinning the samples. A total of 200−500 scans were taken at a rate of approximately 1 scan/s.

Computational Procedures. A SCF−MS−Xα calculation[12,13] was performed on the model compound $[Mo_2(O_2CH)_2(H_2O)_2(OH)_2]$. In the calculation Norman's overlapping atomic sphere radii[14] were assumed to be 88.5% of the atomic number radii. The outer sphere was made tangent to the outer atomic sphere. The α values of the atoms were adopted from Schwarz,[15] and the one for both inner sphere and outer sphere was taken as the valence electron weighted average of the atomic α. The SCF iteration is considered to be converged when the potential shift is less than 10^{-3} Rydberg.

In the model compound, H_2O and OH^- were used to model the phenol and phenoxide groups, respectively. Symmetric hydrogen bonding was assumed for each H_2O/OH^- pair, which leads to C_{2v} point symmetry for the model and an equivalency between H_2O and OH^-. The remaining H atom (H_t) of the H_2O/OH^- group was positioned so that both the bond angle Mo−O−H and dihedral angle Mo−Mo−O−H, respectively, were set to the average of crystallographically determined values for Mo−O−C(phenyl) and Mo−Mo−O−C(phenyl). The THF molecule was omitted from the model since it is only weakly coordinated to the Mo center. The important geometric parameters are Mo−Mo, 2.126 Å; Mo−O (H_2O/OH^-), 2.13 Å; Mo−Mo−O (H_2O/OH^-), 93.56°; Mo−Mo−O−H_t, 145.83°; O−H_t, 0.95 Å; O−H_b, 1.20 Å (H_b is the hydrogen bonded H atom). The geometric parameters for the formate group were the same as those used for $Mo_2(O_2CH)_4$.[16] To meet the convention of *z* being the unique axis of the C_{2v} point group, the master coordinates were defined with the *yz* plane bisecting two bridging formate planes, the *y* axis parallel to the Mo−Mo vector and the *x* axis passing through the center of Mo−Mo linkage. In this setting the Mo−Mo bonding and antibonding orbitals are as follows: δ ($d_{x^2-z^2}(1) + d_{x^2-z^2}(2)$), a_1; δ^* ($d_{x^2-z^2}(1) - d_{x^2-z^2}(2)$), b_2; $\pi(yz)$ ($d_{yz}(1) - d_{yz}(2)$), a_1; $\pi^*(yz)$ ($d_{yz}(1) + d_{yz}(2)$), b_2; $\pi(xy)$ ($d_{xy}(1) - d_{xy}(2)$), b_1; $\pi^*(xy)$ ($d_{xy}(1) + d_{xy}(2)$), a_2; σ ($d_{y^2}(1) + d_{y^2}(2)$), a_1; σ^* ($d_{y^2}(1) - d_{y^2}(2)$), b_2.

Results and Discussion

$[Mo_2(O_2CCF_3)_2(NCCH_3)_6](BF_4)_2$ (1). The preparation of $[Mo_2(O_2CCF_3)_2(NCCH_3)_6](BF_4)_2$ (**1**) proved to be as facile as the syntheses of the previously reported complexes $[Mo_2(O_2CR_3)_2(NCCR_3)_4L_2](BF_4)_2$ (R = H, CH_3; L = $NCCH_3$, O_3SCF_3).[6,7] Unlike the original preparations of this class of compounds in which an excess of Me_3OBF_4 was used, **1** was best prepared with stoichiometric amounts of $[Mo_2(O_2CCF_3)_4]$

(12) Connolly, J. W. D. In *Semiempirical Methods of Electronic Structure Calculation. Part A: Techniques*; Segal, G. A., Ed.; Plenum Press: New York, 1977.
(13) A version of the SCF−Xα program package developed by M. Cook, B. Berstein, and G. G. Stanley was used.
(14) Norman, J. G., Jr. *Mol. Phys.* **1976**, *31*, 1191.
(15) Schwarz, K. *Phys. Rev. B* **1972**, *5*, 2466.
(16) Norman, J. G., Jr.; Kolari, H. J.; Gray, H. B.; Trogler, W. C. *Inorg. Chem.* **1977**, *16*, 987.

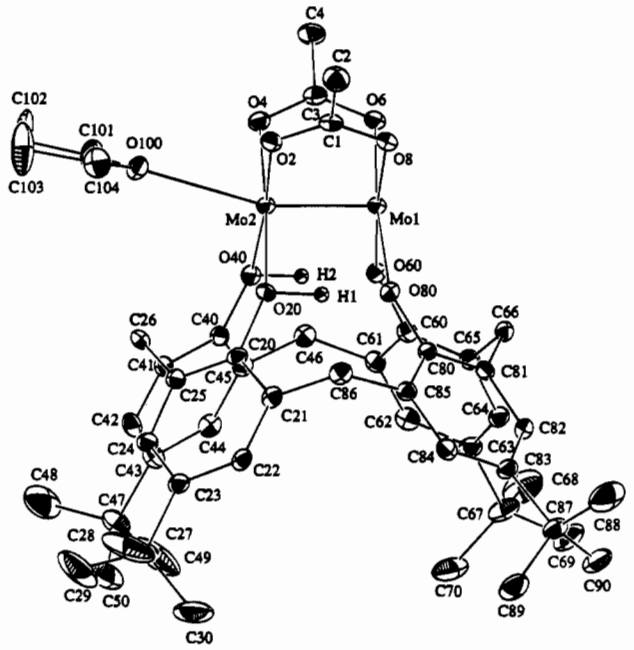

Figure 2. ORTEP drawing of $[Mo_2(O_2CCH_3)_2(H_2$-*p*-*tert*-butylcalix[4]arene)(THF)] (**2**(THF)), showing the 30% thermal ellipsoids for all non-hydrogen atoms and the atom labeling scheme.

and Me_3OBF_4. The reaction of 2 equiv of Me_3OBF_4 in acetonitrile with $[Mo_2(O_2CCF_3)_4]$ proceeded through an array of colors to afford the bright pink product **1** in good yield. Compound **1** can be stored indefinitely under anhydrous conditions, is very soluble in acetonitrile, and is moderately soluble in other polar solvents such as DME and THF. The spectroscopic properties of **1** are similar to those of its analogues. The ^{1}H NMR spectrum shows only one resonance for the $NCCH_3$ groups (δ = 1.96 ppm) at almost the same position as the solvent, suggesting rapid exchange of $NCCH_3$ groups with the solvent. The IR spectrum of **1** in Nujol displays strong peaks (ν = 2323 and 2294 cm^{-1}) corresponding to the C≡N vibrations of the bound acetonitrile ligands. The lowest energy band in the UV−visible absorption spectrum of the product occurs at 528 nm, which is comparable to the lowest energy band at 531 nm in the spectrum of $[Mo_2(O_2CCH_3)_2(NCCH_3)_6](BF_4)_2$, attributed to a metal−metal $\delta \rightarrow \delta^*$ transition.[7] Analytical results for **1** correspond to the loss of one acetonitrile ligand, consistent with elemental analyses of analogues of **1**[6,7] and the solvent lability demonstrated by ^{1}H NMR spectroscopy mentioned above.

Preparation of $[Mo_2(O_2CCH_3)_2(H_2$-*p*-*tert*-butylcalix[4]arene)] (2), $[Mo_2(O_2CCF_3)_2(H_2$-*p*-*tert*-butylcalix[4]arene)] (3), $[Mo_2(O_2CCH_3)_2(H_2$-calix[4]arene)] (4), and $[Mo_2(O_2CCF_3)_2(H_2$-calix[4]arene)] (5). The complexes $[Mo_2(O_2CR_3)_2(NCCH_3)_6](BF_4)_2$ (R = CH_3, CF_3 (**1**)) proved to be useful starting materials for the preparation of calixarene-substituted quadruply bonded dimolybdenum products **2**−**5**. The labile acetonitrile ligands were readily displaced by doubly-deprotonated calixarene macrocycles. Reaction progress was monitored in THF by the disappearance of the insoluble starting material. The neutral products were purified by extraction into nonpolar solvents and filtration to remove salts and residual starting materials. The products are extremely air-sensitive in the solid state as well as in solution.

One advantage in using calix[4]arene ligands in transition metal chemistry is the characteristic ^{1}H NMR spectra of their diamagnetic complexes.[1] Metal incorporation and the overall symmetry of the molecule are immediately apparent from the shape and number of doublets corresponding to the methylene protons of the calix[4]arene ligand. The presence of four sets of sharp methylene doublets in the ^{1}H NMR spectra of **2**−**5** indicated products with approximately 2-fold symmetry and geometrically fixed calixarene ligands. In THF-d_8, the NMR spectra of **2**−**5** contained broad peaks at 1.78 and 3.63 ppm, only slightly downfield of the chemical shift of the solvent, suggesting axial coordination of THF by the complexes in solution. This coordination was confirmed in the solid state by X-ray crystallography.

Table 3. Selected Interatomic Bond Distances (Å) and Angles (deg) for $[Mo_2(O_2CCH_3)_2(H_2$-*p*-*tert*-butylcalix[4]arene)(THF)]·C_6H_6 ((**2**)(THF)·C_6H_6)[a]

Bond Distances (Å)			
Mo(1)−Mo(2)	2.1263(6)	O(2)−C(1)	1.271(5)
Mo(1)−O(6)	2.081(3)	O(4)−C(3)	1.261(5)
Mo(1)−O(8)	2.083(3)	O(6)−C(3)	1.274(5)
Mo(1)−O(60)	2.120(3)	O(8)−C(1)	1.273(5)
Mo(1)−O(80)	2.107(3)	O(20)−C(20)	1.376(5)
Mo(2)−O(2)	2.082(3)	O(20)−H(1)	1.06(5)
Mo(2)−O(4)	2.095(3)	O(40)−C(40)	1.373(5)
Mo(2)−O(20)	2.148(3)	O(40)−H(2)	0.99(5)
Mo(2)−O(40)	2.144(3)	O(60)−C(60)	1.380(5)
O(100)−Mo(2)	2.552(3)	O(80)−C(80)	1.368(5)
Bond Angles (deg)			
Mo(2)−Mo(1)−O(6)	92.12(9)	O(2)−Mo(2)−O(4)	92.3(1)
Mo(2)−Mo(1)−O(8)	91.77(9)	O(2)−Mo(2)−O(20)	86.9(1)
Mo(2)−Mo(1)−O(60)	93.35(8)	O(2)−Mo(2)−O(40)	175.0(1)
Mo(2)−Mo(1)−O(80)	93.73(9)	O(4)−Mo(2)−O(20)	176.5(1)
O(6)−Mo(1)−O(8)	90.7(1)	O(4)−Mo(2)−O(40)	89.3(1)
O(6)−Mo(1)−O(60)	89.8(1)	O(20)−Mo(2)−O(40)	91.2(1)
O(6)−Mo(1)−O(80)	174.0(1)	Mo(2)−O(2)−C(1)	118.8(3)
O(8)−Mo(1)−O(60)	174.8(1)	Mo(2)−O(4)−C(3)	118.3(3)
O(8)−Mo(1)−O(80)	88.0(1)	Mo(1)−O(6)−C(3)	117.1(3)
O(60)−Mo(1)−O(80)	90.9(1)	Mo(1)−O(8)−C(1)	117.6(3)
Mo(1)−Mo(2)−O(2)	90.67(9)	Mo(2)−O(20)−C(20)	145.8(3)
Mo(1)−Mo(2)−O(4)	90.38(9)	Mo(2)−O(40)−C(40)	145.4(3)
Mo(1)−Mo(2)−O(20)	93.08(9)	Mo(1)−O(60)−C(60)	143.7(3)
Mo(1)−Mo(2)−O(40)	94.07(9)	Mo(1)−O(80)−C(80)	146.4(3)

[a] See Figure 2 for atom labeling scheme. Estimated standard deviations in the least significant figure are given in parentheses.

Structural Results. $[Mo_2(O_2CCH_3)_2(H_2$-*p*-*tert*-butylcalix[4]arene)(THF)]·C_6H_6 (2(THF)·C_6H_6). The solid state structure of this compound was revealed in an X-ray diffraction study. An ORTEP diagram of **2**(THF) is shown in Figure 2, and selected bond distances and angles are given in Table 3. The molecule has no crystallographically imposed symmetry, and no disorder was encountered during the structure refinement. The quadruply-bonded dimolybdenum core of **2**(THF) is bridged by two bidentate acetate ligands and coordinated in a tetradentate fashion by the doubly-deprotonated calixarene macrocycle. This tetradentate bridging coordination mode is rather unusual, although similar to the bridging bis bidentate coordination of the tetraazamacrocyclic ligand H_2TMTAA (5,7,12,14-tetramethyldibenzo[*b*,*i*][1,4,8,11]tetraazacyclotetradecine) in $[Mo_2(O_2CCH_3)_2$(TMTAA)].[17] In both molecules, the Mo$\equiv$Mo core is spanned by the macrocyclic ligands as well as by two bridging carboxylate ligands. A more common binding motif for such tetradentate ligands, which occurs in the complexes [{Mo(TMTAA)}$_2$],[18,19] [{Mo(acacen)}$_2$],[20] [{Mo(TPP)}$_2$],[21] [{Mo(OEP)}$_2$],[22] and [{Mo(TOEP)}$_2$],[23] has one macrocycle individually coordinating each molybdenum atom, leaving the Mo$\equiv$Mo core unbridged.

(17) Kerbaol, J. M.; Furet, E.; Guerchais, J. E.; Le Mest, Y.; Saillard, J. Y.; Sala-Pala, J.; Toupet, L. *Inorg. Chem.* **1993**, *32*, 713.
(18) Mandon, D.; Giraudon, J.-M.; Toupet, L.; Sala-Pala, J.; Guerchais, J. E. *J. Am. Chem. Soc.* **1987**, *109*, 3490.
(19) Cotton, F. A.; Czuchajowska, J.; Feng, X. *Inorg. Chem.* **1990**, *29*, 4329.

Table 4. Structural Parameters for Some $[Mo_2]^{4+}$ Complexes

compound	bond distances (Å)	
	Mo−Mo	average Mo−O
$[Mo_2(O_2CCH_3)_2(H_2$-*p*-*tert*-butylcalix[4]arene)(THF)] (**2**)(THF)	2.1263 (6)	2.11 (O_{calix}) 2.15 (HO_{calix}) 2.08 ($O_{acetate}$)
$[Mo_2(O_2CCH_3)_4]$[48]	2.0934 (8)	2.12
$[Mo_2(O_2CCF_3)_4]$[10]	2.090 (4)	2.06
$[Mo_2(O_2CCH_3)_2(TMTAA)]$[17,a]	2.106 (1)	2.12
$[Mo_2(O$-*i*-Pr$)_4($HO-*i*-Pr$)_4]$[27]	2.110 (3)	2.09 (OR) 2.17 (HOR)
$[Mo_2(O$-*i*-Pr$)_4(py)_4]$[27]	2.195 (1)	2.03
$[Mo_2(OC_6F_5)_4(HNMe_2)_4]$[49]	2.140 (2)	2.07
$[Mo_2(OC_6F_5)_4(PMe_3)_4]$[50]	2.146 (2)	2.09

[a] TMTAA = 5,7,12,14-tetramethyldibenzo[*b*,*i*][1,4,8,11]tetraazacyclotetradecine.

The Mo−Mo distance of 2.1263 (6) Å and the eclipsed geometry of the Mo_2O_8 moiety are indicative of a quadruple bond.[24,25] The Mo≡Mo separation as well as the Mo−O_{ligand} distances of **2**(THF) can be compared with the relevant structural features of some other $[Mo_2]^{4+}$ complexes having carboxylate, alkoxide, or phenoxide ligands. As shown in Table 4, the metal−metal distance in **2**(THF) is about 0.03 Å longer than the corresponding distance in the carboxylate complexes $[Mo_2(O_2CCH_3)_4]$ and $[Mo_2(O_2CCF_3)_4]$. The Mo≡Mo separation and Mo−O_{ligand} distances of **2**(THF) are more similar to corresponding values in the alkoxide and phenoxide complexes listed in Table 4. It was proposed for these latter compounds[26,27] that there are repulsive interactions between electrons in the filled p_π phenol and phenoxide oxygen atomic orbitals and those in the filled Mo−Mo δ orbital. Such an interaction is possible in the calixarene bridging mode found in **2**(THF)·C_6H_6, for which the average Mo−O−C(calix) angle is 145°, consistent with approximate sp^2 hybridization of the oxygen atoms. A detailed molecular orbital picture of **2** was revealed by SCF−Xα studies, as discussed below.

The hydrogen atoms H(1) and H(2), which were located and refined without difficulty, participate in asymmetrical hydrogen bonding interactions (O(20)−H(1) = 1.06 (5), H(1)···O(80) = 1.32 (6) Å; O(40)−H(2) = 0.99 (5), H(2)···O(60) = 1.43 (5) Å) parallel to the Mo≡Mo vector. These hydrogen bonds are extremely strong (O(40)···O(60) = 2.403 (4) Å, O(20)···O(80) = 2.380 (4) Å) compared to those in the related complexes $[M_2(O$-*i*-Pr$)_8($HO-*i*-Pr$)_2]$ (M = Zr, Ce), for which the O···O separation was 2.76−2.78 Å.[28,29] The metal−metal distances in these latter complexes (3.50 Å for M = Zr and 3.77 Å for M = Ce) indicate nonbonding interactions. By contrast, in the quadruply-bonded dimolybdenum complexes $[Mo_2(O$-*i*-Pr$)_4($HO-*i*-Pr$)_4]$ and $[Mo_2(O$-c-Pen$)_4($HO-c-Pen$)_4]$ the O···O distances were also quite short, *ca.* 2.40 Å.[27] The hydrogen atoms were not located in these structures. In solution, complexes **2**−**5** show only one resonance for the hydrogen bonded hydroxyl protons in the ^{1}H NMR spectrum, ≈16.9 ppm. By comparison, the hydroxyl proton in the $[Mo_2(OR)_4(HOR)_4]$ complexes resonates at 12.5 ppm.[27] These chemical shifts are significantly downfield of the δ = 6.3 ppm shift of the hydroxyl protons of $[Zr_2(O$-*i*-Pr$)_8($HO-*i*-Pr$)_2]$,[28,29] in which the metals are not directly bonded to one another. These differences reflect the large diamagnetic anisotropy of the Mo≡Mo bond.[30,31]

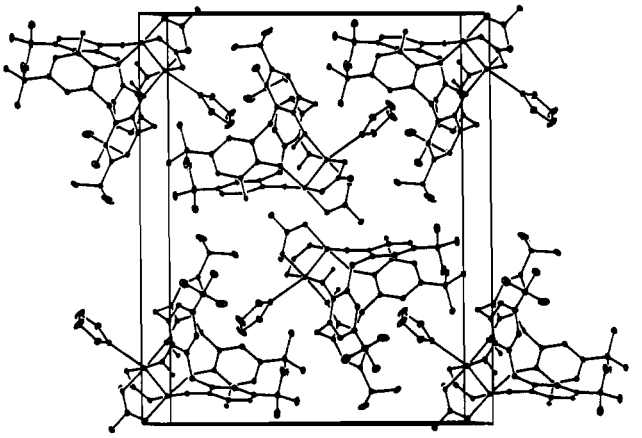

Figure 3. Crystal packing of $[Mo_2(O_2CCH_3)_2(H_2$-*p*-*tert*-butylcalix[4]arene)(THF)] ((**2**)(THF)). Benzene molecules in the lattice were omitted for clarity.

As shown in Figure 2, a THF molecule is bound axially to Mo(2) of **2** in the solid state. Although axial ligation to the metal−metal quadruple bond is well precedented, it is more common in dichromium compounds, where there are typically two such ligands rather than one.[5] The Mo−O(THF) distance of 2.552 (3) Å may be compared to that of other reported dimolybdenum complexes with axially ligated THF molecules. Examples include $[Mo_2(S_2COC_2H_5)_4(THF)_2]$ (Mo−O(THF) = 2.795 (1) Å),[32] $[Mo_2\{(2,6\text{-}Me_2C_6H_3)NC(H)O\}_4(THF)_2]$ (Mo−O(THF) = 2.564 (5) Å),[33] $[Mo_2\{(2,6\text{-}Me_2C_6H_3)N\}_2CCH_3\}_2(O_2CCH_3)_2(THF)_2]$ (Mo−O(THF) = 2.709 (6) Å),[34] and $[Mo(C_5H_3O_2S)_4(THF)_2]$ (Mo−O(THF) = 2.593 (5) Å).[35] A noteworthy feature of the extended lattice of **2**(THF) can be seen in the packing diagram (Figure 3). The axially-coordinated THF molecule of one complex is included in the pocket of the calixarene in the neighboring complex. Inclusion of guests in the *p*-*tert*-butylcalix[4]arene macrocycle has been seen in the solid state for a variety of neutral molecules, such as toluene,[3a] benzene and xylene,[36] and anisole.[36] This property has been explained in part by invoking alkyl−phenyl interactions.[37] In the case of **2**(THF), the calixarene macrocycle has aided in the organization of an intimately connected extended structure, as illustrated in Figure 4. Each complex is weakly coordinated to the neighboring molecules through axial interactions via Mo−O bonds with Mo···O distances of 3.45 Å and the axial ligation of a THF molecule included in the next calixarene basket. The

(20) Pennesi, G.; Floriani, C.; Chiesi-Villa, A.; Guastini, C. *J. Chem. Soc., Chem. Commun.* **1988**, 350.
(21) Yang, C.-H.; Dzugan, S. J.; Goedken, V. L. *J. Chem. Soc., Chem. Commun.* **1986**, 1313.
(22) Tait, C. D.; Garner, J. M.; Collman, J. P.; Sattelberger, A. P.; Woodruff, W. H. *J. Am. Chem. Soc.* **1989**, *111*, 9072.
(23) Collman, J. P.; Garner, J. M.; Hembre, R. T.; Ha, Y. *J. Am. Chem. Soc.* **1992**, *114*, 1292.
(24) Cotton, F. A.; Curtis, N. F.; Harris, C. B.; Johnson, B. F. G.; Lippard, S. J.; Mague, J. T.; Robinson, W. R.; Wood, J. S. *Science* **1964**, *145*, 1305.
(25) Cotton, F. A. *Inorg. Chem.* **1965**, *4*, 334.
(26) Chisholm, M. H.; Folting, K.; Huffman, J. C.; Tatz, R. J. *J. Am. Chem. Soc.* **1984**, *106*, 1153.
(27) Chisholm, M. H.; Folting, K.; Huffman, J. C.; Putilina, E. F.; Streib, W. E.; Tatz, R. J. *Inorg. Chem.* **1993**, *32*, 3771.
(28) Vaarstra, B. A.; Huffman, J. C.; Gradeff, P. S.; Hubert-Pfalzgraf, L. G.; Daran, J.-C.; Parraud, S.; Yunlu, K.; Caulton, K. G. *Inorg. Chem.* **1990**, *29*, 3126.
(29) Huggins, B. A.; Ellis, P. D.; Gradeff, P. S.; Vaarstra, B. A.; Yunlu, K.; Huffman, J. C.; Caulton, K. G. *Inorg. Chem.* **1991**, *30*, 1720.
(30) San Filippo, J., Jr. *Inorg. Chem.* **1972**, *11*, 3140.
(31) Cotton, F. A.; Kitagawa, S. *Polyhedron* **1988**, *7*, 1673.
(32) Ricard, L.; Karagiannidis, P.; Weiss, R. *Inorg. Chem.* **1973**, *12*, 2179.
(33) Cotton, F. A.; Ilsley, W. H.; Kaim, W. *Inorg. Chem.* **1980**, *19*, 3586.
(34) Cotton, F. A.; Ilsley, W. H.; Kaim, W. *Inorg. Chem.* **1981**, *20*, 930.
(35) Cotton, F. A.; Falvello, L. R.; Reid, A. H., Jr.; Roth, W. J. *Acta Crystallogr.* **1990**, *C46*, 1815.
(36) Coruzzi, M.; Andreetti, G. D.; Bocchi, V.; Pochini, A.; Ungaro, R. *J. Chem. Soc., Perkin Trans. 2* **1982**, 1133.
(37) Andreetti, G. D.; Ori, O.; Ugozzoli, F.; Alfieri, C.; Pochini, A.; Ungaro, R. *J. Inclusion Phenom.* **1988**, *6*, 523.

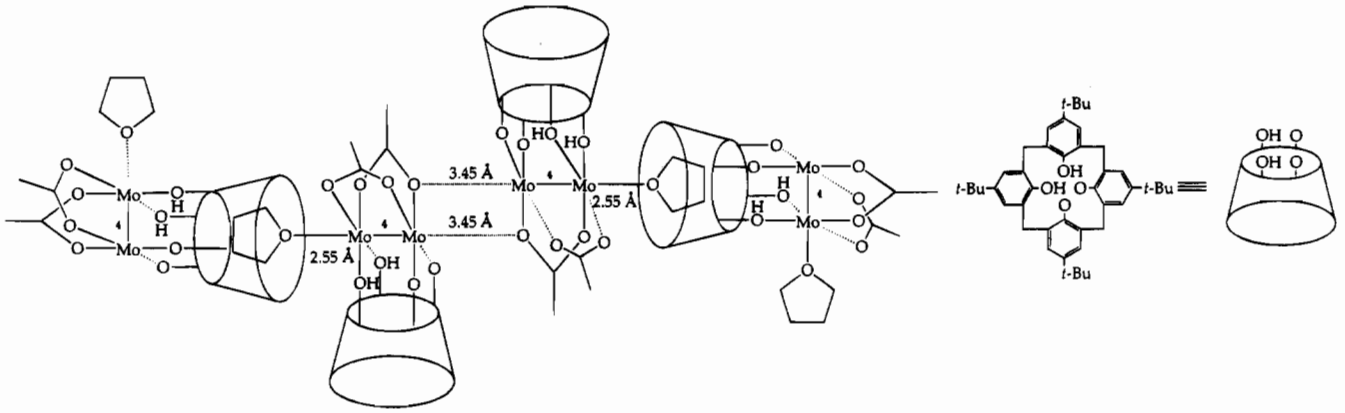

Figure 4. Schematic drawing of the extended lattice contacts in **2**(THF).

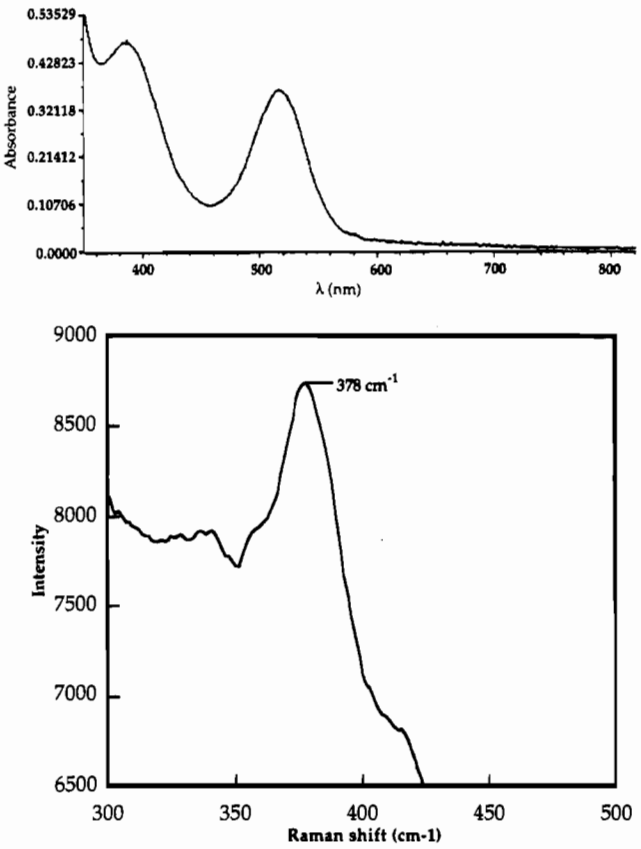

Figure 5. UV−visible (top) and resonance Raman (bottom) spectra of $[Mo_2(O_2CCH_3)_2(H_2$-*p*-*tert*-butylcalix[4]arene)] (**2**). The resonance Raman spectrum (250−500 cm^{-1}) was recorded in THF solution with 514.5-nm excitation.

closest *endo*-calix interaction of 3.50 Å occurs between C(102) of the THF molecule and the plane of the phenyl ring C(20)−C(25). This value is similar to that found in other calixarene inclusion complexes.[38,39]

Electronic Spectra of 2−5. Compounds **2−5** are all highly colored, displaying various shades of red and orange, and their solution UV−visible absorption spectra share common features. The spectrum of **2** in THF is shown as an example at the top of Figure 5. The lowest energy transitions for **2−5** occur at λ_{max} (ϵ, M^{-1} cm^{-1}) values of 514 (875), 530 (1005), 512 (591), and 528 (719) nm, respectively. These values are similar to the lowest energy transitions seen for other $[Mo_2]^{4+}$ complexes, such as $[Mo_2(O_2CCH_3)_4]$ (λ_{max}, 435 nm; ϵ, 150 M^{-1} cm^{-1})[40] and $[Mo_2(O_2CCF_3)_4]$ (λ_{max}, 435 nm; ϵ, 120 M^{-1} cm^{-1}),[10] which were assigned as metal−metal $\delta \rightarrow \delta^*$ transitions. The experimentally observed shift to lower energies for this band in the calixarene substituted products **2−5** is consistent with the results of SCF−Xα calculations. These calculations reveal significant antibonding contributions from the lone pairs of the phenol and phenoxide moieties of the calixarene macrocycle to the Mo−Mo δ orbital, details of which are discussed below. Moreover, the intensities of the $\delta \rightarrow \delta^*$ transitions of **2−5** are considerably larger than the intensities of the corresponding bands in $[Mo_2(O_2CCH_3)_4]$ and $[Mo_2(O_2CCF_3)_4]$. This result is also consistent with the effects of ligand orbital mixing with δ, δ^* orbitals.[41] Higher energy bands observed in the electronic spectra of **2−5** (see Experimental Section) are due to ligand-to-metal charge transfer.

Resonance Raman Spectra of 2−5. These compounds all display a band in the 300−500-cm^{-1} region of their Raman spectra, as illustrated at the bottom of Figure 5 for **2** dissolved in THF. The position, intensity, and breadth of the bands at 378, 360, 379, and 357 cm^{-1} for **2−5**, respectively, are characteristic of the totally symmetric ν_{Mo-Mo} vibration.[42] For complexes **2−5**, which have approximate C_{2v} symmetry, the totally symmetric vibration belongs to the A_1 irreducible representation.

The choice of excitation at 514.5 nm in the Raman studies of **2−5** was made to coincide with their $\delta \rightarrow \delta^*$ transitions, providing resonance enhancement of the bands. Resonance enhancement of the Raman spectra for quadruply-bonded Mo−Mo species was first observed in 1973[43] and since then has been widely utilized for the study of metal−metal bonded species.[42] In general, the frequency of the Raman vibration increases with the order of the bond being investigated.[44,45] In the case of quadruply-bonded dimolybdenum complexes, the assignment of the A_1 vibration as molybdenum−molybdenum stretching is only a rough approximation, since there is most likely also some ligand character. A comparison of Raman and infrared frequencies for the A_1 vibration and Mo−Mo bond distances for some dimolybdenum complexes, including **2−5**, is made in Table 5. These data suggest that, although there is not a strict correlation between Raman frequencies and Mo−Mo bond distances,

(38) Gutsche, C. D. *Top. Curr. Chem.* **1984**, *123*, 1.
(39) *Calixarenes: A Versatile Class of Macrocyclic Compounds*; Vicens, J., Böhmer, V., Eds.; Kluwer Academic Publishers: Dordrecht, The Netherlands, 1991; Vol. 3.
(40) Martin, D. S.; Newman, R. A.; Fanwick, P. E. *Inorg. Chem.* **1979**, *18*, 2511.
(41) Hopkins, M. D.; Gray, H. B.; Miskowski, V. M. *Polyhedron* **1987**, *6*, 705.
(42) Clark, R. J. H.; Dines, T. J. *Angew. Chem., Int. Ed. Engl.* **1986**, *25*, 131.
(43) Angell, C. L.; Cotton, F. A.; Frenz, B. A.; Webb, T. R. *J. Chem. Soc., Chem. Commun.* **1973**, 399.
(44) Long, T. V.; Plane, R. A. *J. Chem. Phys.* **1965**, *43*, 457.
(45) Quicksall, C. O.; Spiro, T. G. *Inorg. Chem.* **1970**, *9*, 1045.

Table 5. Raman and Infrared Frequencies (cm^{-1}) and Bond Distances (Å) for Some $[Mo_2]^{4+}$ Complexes

compound	frequency (cm^{-1}) Raman	infrared	Mo−Mo distance (Å)
$[Mo_2(O_2CCH_3)_4]$	404[51-54]		2.0934 (8)[48]
$[Mo_2(O_2CCF_3)_4]$	397[10,52]		2.090 (4)[10]
$[Mo_2(O_2CCH_3)_2$(H$_2$-*p*-*tert*-butylcalix[4]arene)(THF)]((**2**)(THF))	378[a]	381	2.1263 (6)
$[Mo_2(O_2CCH_3)_2$(H$_2$-calix[4]arene)] (**4**)	379[a]	376	
$[Mo_2(O_2CCF_3)_4(py)_2]$	367[52,55]		2.129 (2)[55]
$[Mo_2(O_2CCF_3)_2$(H$_2$-*p*-*tert*-butylcalix[4]arene)] (**3**)	360[a]	358	
$[Mo_2(O_2CCF_3)_2$(H$_2$-calix[4]-arene)] (**5**)	357[a]	358	
$[(enH_2)_2(Mo_2Cl_8)]\cdot 2H_2O$	348[43,56]		2.134 (1)[57]
$[K_4Mo_2Cl_8]\cdot 2H_2O$	345[43,56]		2.139 (4)[58]

[a] Spectra were recorded as 0.14 M solutions in THF.

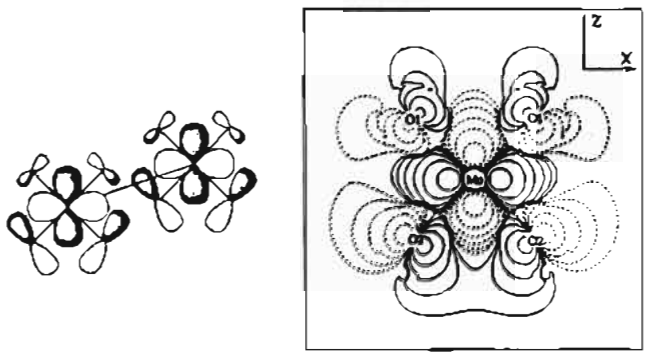

(a) (b)

Figure 6. Ligand−metal interaction in the δ orbital: (a) schematic drawing; (b) contour plot of the δ orbital projected on the plane parallel to *xz* and containing one Mo center (the inset shows the choice of coordinate system).

2−**5** occupy predictable positions in a discernible pattern. According to the series in Table 5, a higher frequency of the A_1 vibration Raman band corresponds to a shorter Mo≡Mo bond. Axial ligands can also have a substantial effect on the observed frequency of the A_1 vibration, lowering the value by 30−40 cm^{-1}, as seen by comparing ν_{Mo-Mo} of 397 cm^{-1} for $[Mo_2(O_2CCF_3)]$ and 367 cm^{-1} for $[Mo_2(O_2CCF_3)(py)_2]$ in Table 5. ^1H NMR spectroscopic and the solid state structural evidence indicate axial ligation of **2**−**5** by THF, and this coordination must also be taken into account in evaluating the resonance Raman spectra of **2**−**5** in THF solution. The products **2**−**5**, unlike many of the published quadruply-bonded dimolybdenum complexes, do not have centers of inversion. The rule of mutual exclusion therefore does not apply,[46] and the A_1 vibration of **2**−**5** is also IR active, giving rise to stretches at 381, 358, 376, and 358 cm^{-1}, respectively.

Results of Computational Studies. Although there are many SCF−Xα studies of the quadruply bonded Mo_2 species,[5] the uniqueness of $[Mo_2(O_2CCH_3)_2$(*p*-*tert*-butylcalix[4]arene)] (**2**), both in terms of its coordination geometry and the nature of the ligand, calls for an independent study. The energy levels and charge distributions of the upper valence molecular orbitals of the converged SCF iteration are listed in Table 6; the table omits both low energy and ligand-dominant MO's (C−H, C−O, and O−H σ bonds) since they are not of particular interest in the present context. The relative distribution of metal−metal bonding and antibonding orbitals is identical to that of $[Mo_2(formate)_4]$,[16] and these orbitals are assigned, in ascending order of energy, as $8a_1$ and $10a_1$ (σ), $9b_1$ and $10b_1$ (π_{xy}), $11a_1$ (π_{yz}), $12a_1$ (δ, HOMO), $9b_2$ (δ^*, LUMO), $9a_2$ (π_{xy}^*), $10b_2$ (π_{yz}^*), and $11b_2$. Both the σ and π_{xy} orbitals are split into two MO's owing to symmetry-allowed mixing with Mo−O σ bonding orbitals, which were also identified in the Xα calculation of $[Mo_2(formate)_4]$.[16] Since there is no filled metal−metal antibonding orbital, the existence of a Mo−Mo quadruple bond is unambiguous. Although the electronic structure of **2** is generally similar to that of $[Mo_2(formate)_4]$, there are a couple of noteworthy distinctions.

First, the HOMO−LUMO gap (1.03 eV) is significantly smaller than the one calculated for $[Mo_2(formate)_4]$ (1.51 eV).[16] This result arises from an antibonding contribution from the lone pair of the phenoxy group (13%) in the δ orbital. The antibonding nature of this interaction is obvious from both the schematic drawing (Figure 6a) and the contour plot (Figure 6b, viewed along the Mo−Mo vector) of the δ orbital. On the other hand, the similar contribution from the carboxylate oxygen atoms is very small, as evidenced by both the charge contribution (1%) and the contour plot. Meanwhile, the δ^* orbital of **2** experiences about the same degree of antibonding interaction as $[Mo_2(formate)_4]$ from the viewpoint of charge contribution (16% oxygen contribution in the former and 14% in the latter). Therefore, the strong π donation of the phenoxy group is solely responsible for the pronounced destabilization of the δ orbital in **2**, which in turn yields a reduced $\delta-\delta^*$ gap (compared with $[Mo_2(formate)_4]$). This reduction is consistent with the above-mentioned red-shift of the $\delta-\delta^*$ transition in the UV−visible spectrum.

Second, the phenoxy ligand contribution to Mo−Mo π_{xy} orbital is so large that there are two MOs, $9b_1$ and $10b_1$, with essentially equal contributions from both MoMo π_{xy} orbitals and oxygen p orbitals. On the other hand, the π_{yz} orbital ($11a_1$) contains much less oxygen contribution. The difference between π_{xy} and π_{yz} is mainly due to the choice of the coordinate system. It is, however, the nature of the ligand contribution in π_{xy} that we are interested in. In contrast to the previously suggested lone-pair π donation to the Mo−Mo π orbital in $[Mo_2(O\text{-}i\text{-}Pr)_4(HO\text{-}i\text{-}Pr)_4]$,[27] the lone pair orbital of the phenoxy group does not play a significant role. Instead, the symmetry-allowed σ type overlap between π_{xy} and the *p* type oxygen orbital is responsible. This overlap can be clearly seen in Figures 2 and 3 of ref 16, where a head-to-head overlap along the Mo−O linkage is obvious, although it was termed a Mo−O π interaction in the original paper. A qualitative drawing of the overlap between the MoMo π_{xy} and the symmetry adapted linear combination of the lone pair orbitals from the phenoxy group (supplementary material, Figure S4) also indicates a minimal interaction. Compared with $[Mo_2(formate)_4]$, the much higher percentage of oxygen contribution in the π_{xy} orbital also reflects the fact that phenoxide is a stronger σ base.

Finally, we wish to point out that although the conjugation involving the phenyl ring and the lone pair of the oxygen atom may influence the π donating ability of the phenoxy group, a Fenske−Hall calculation of **2** with a full calixarene ligand reveals that the contribution from the π orbital of the phenyl ring is negligible.[47] This result justifies the omission of the phenyl rings in the current Xα calculation.

(46) Cotton, F. A. *Chemical Applications of Group Theory;* 3rd ed.; Wiley: New York, 1990.
(47) Ren, T. Unpublished results.
(48) Cotton, F. A.; Mester, Z. C.; Webb, T. R. *Acta Crystallogr.* **1974**, *B30*, 2768.
(49) Abbott, R. G.; Cotton, F. A.; Falvello, L. R. *Inorg. Chem.* **1990**, *29*, 514.
(50) Cotton, F. A.; Wiesinger, K. J. *Inorg. Chem.* **1991**, *30*, 750.
(51) Bratton, W. K.; Cotton, F. A.; Debeau, M.; Walton, R. A. *J. Coord. Chem.* **1971**, *1*, 121.

Table 6. Upper Valence Molecular Orbitals (MO) of $Mo_2(O_2CH)_2(H_2O)_2(OH)_2$

MO	*E*(eV)	assignment	MO composition[a] (%)				angular distribution[b] of Mo contribution
			Mo	O(1)	O(2)	C	
$11b_2$	−3.367	Mo−Mo σ^*	90	5	5	0	85% D, 14% P, 1% S
$11b_1$	−3.454	antibonding of $9b_1$ and $10b_1$	71	17	10	0	100% D
$10b_2$	−4.512	Mo−Mo π^*_{yz}	93	1	5	0	99% D, 1% P
$9a_2$	−4.524	Mo−Mo π^*_{xy}	93	1	5	0	99% D, 1% P
$9b_2$	−5.845	Mo−Mo δ^*, LUMO	84	7	9	0	100% D
$12a_1$	−6.874	Mo−Mo δ, HOMO	82	1	13	3	100% D
$8a_2$	−8.539		5	2	93	0	
$8b_2$	−8.625		5	2	93	0	
$7a_2$	−8.885		2	9	89	0	
$11a_1$	−9.088	Mo−Mo π_{yz}	86	9	3	0	97% D, 2% S
$10b_1$	−9.125	Mo−Mo π_{xy} and Mo−O σ	52	10	36	0	100% D
$9b_1$	−9.263	Mo−O σ and Mo−Mo π_{xy}	48	3	46	1	97% D, 3% P
$7b_2$	−9.569		6	16	78	0	
$10a_1$	−9.925	Mo−O σ, Mo−Mo σ	42	43	4	4	65% D, 9% P, 25%
$6a_2$	−10.046		0	98	1	0	
$9a_1$	−10.210		16	9	73	1	
$6b_2$	−10.255		6	88	5	0	
$5a_2$	−10.545		11	78	9	1	
$8b_1$	−10.700		13	50	22	4	
$5b_2$	−10.867		13	78	8	0	
$8a_1$	−11.216	Mo−Mo σ, Mo−O σ	60	9	25	1	88% D, 5% P, 8% S
$7b_1$	−12.540		2	75	2	21	

[a] O(1) is the formate oxygen, and O(2) is the phenoxy oxygen. [b] Only given when the MO contains more than 30% Mo contribution.

Conclusions

Four novel calix[4]arene complexes of the dimolybdenum quadruple bond have been prepared by reacting doubly-deprotonated calix[4]arene and *p-tert*-butylcalix[4]arene with the labile complexes $[Mo_2(O_2CCH_3)_2(NCCH_3)_6](BF_4)_2$ and $[Mo_2(O_2CCF_3)_2(NCCH_3)_6](BF_4)_2$ (**1**), a new and effective starting material for quadruply-bonded dimolybdenum compounds. The geometry and electronic structure of the products $[Mo_2(O_2CCH_3)_2(H_2$-*p-tert*-butylcalix[4]arene)] (**2**), $[Mo_2(O_2CCF_3)_2(H_2$-*p-tert*-butylcalix[4]arene)] (**3**), $[Mo_2(O_2CCH_3)_2(H_2$calix[4]arene)] (**4**), and $[Mo_2(O_2CCF_3)_2(H_2$-calix[4]arene)] (**5**) were probed by ^1H NMR spectroscopy, X-ray crystallography, and electronic and vibrational spectroscopy. These studies indicate that the tetradentate bridging mode for the calixarene in this class of complexes allows for interaction of filled ligand orbitals with the Mo−Mo δ bond. This result is supported by SCF−Xα calculations, revealing details of the bonding in **2**. In the solid state, $[Mo_2(O_2CCH_3)_2(H_2$-*p-tert*-butylcalix[4]arene)(THF)]·C_6H_6 has an intimately connected extended structure organized in part by the inclusion capability of the *p-tert*-butylcalix[4]arene macrocycle.

Acknowledgment. This work was supported by a grant from the National Science Foundation. The authors thank Dr. Xuejun Feng of Texas A&M University for generating Figure 6b and for helpful discussions regarding the Xα calculation. The resonance Raman spectroscopy was carried out in the George R. Harrison Spectroscopy Laboratory at the Massachusetts Institute of Technology.

Supporting Information Available: Tables of anisotropic thermal parameters and complete interatomic bond distances and angles for $[Mo_2(O_2CCH_3)_2(H_2$-*p-tert*-butylcalix[4]arene)] (**2**) and figures of the 300−500-cm^{-1} region of the Raman spectra of **3**−**5** and of the combination of MoMo p_{xy} orbital and the b_1 symmetry SALC showing minimal overlap (12 pages). Ordering information is given on any current masthead page.

IC950287E

(52) San Filippo, J., Jr.; Sniadoch, H. J. *Inorg. Chem.* **1973**, *12*, 2326.
(53) Ketteringham, A. P.; Oldham, C. *J. Chem. Soc., Dalton Trans.* **1973**, 1067.
(54) Clark, R. J. H.; Hempleman, A. J.; Kurmoo, M. *J. Chem. Soc., Dalton Trans.* **1988**, 973.
(55) Cotton, F. A.; Norman, J. G., Jr. *J. Am. Chem. Soc.* **1972**, *94*, 5697.
(56) Clark, R. J. H.; Franks, M. L. *J. Am. Chem. Soc.* **1975**, *97*, 2691.
(57) Brencic, J. V.; Cotton, F. A. *Inorg. Chem.* **1969**, *8*, 2698.
(58) Brencic, J. V.; Cotton, F. A. *Inorg. Chem.* **1969**, *8*, 7.